Draft version April 7, 2025
Typeset using LaTeX **twocolumn** style in AASTeX631

# Constraint result to the self-interacting dark matter model without dark energy in cosmology

Yixuan Zhu[1]

[1] *Department of Astronomy, Beijing Normal University. Beijing 100875. PR China*

ABSTRACT

## 1. INTRODUCTION

The standard Λ-Cold Dark Matter (ΛCDM) model has been successful in explaining the accelerated expansion of the Universe (Riess et al. (1998); Perlmutter et al. (1999)), from the cosmic microwave background (CMB) anisotropies (Bennett et al. (1996)) to the measurement of baryon acoustic oscillations (BAO; Eisenstein et al. (2005)). However, there are also many alternative models that have been proposed to explain, such as the dynamical dark energy models and the modified gravity models.

It has been shown that dark matter self-interaction could distribute to the accelerated expansion without dark energy component. According to the Boltzmann formalism, the disequilibrium between dark matter particle creation and annihilation processes would creat an effective source term making negative pressure just like the dark energy. Basilakos & Plionis (2009) investigated the analytical solutions for the simple interacting dark matter (IDM) model, and find that the effective annihilation term is much smaller than the results given by the general methods. The gravitational matter creation model is mathematically equivalent to one case of the IDM models.

In this paper, we use the newly revised data from $H(z)$, supernovae Ia, quasars and baryon acoustic oscillation by using the Markov chain Monte Carlo (MCMC) method. The result gives that the lower limit of the interacting dark matter particle mass is about 1 eV.

## 2. THE BASIC EQUATIONS IN THE IDM MODEL

We assume that the total density of the cosmic fluid obeys the collisional Boltzmann equation

$$\dot{\rho} + 3H\rho + \kappa\rho^2 - 2\Psi = 0, \tag{1}$$

where $\rho$ is the total energy-density of the cosmic fluid, containing dark matter, baryons, and any type of exotic energy, $\Psi$ is the rate of creation of DM particle pairs, and the annihilation parameter $\kappa(\geq 0)$ is given by:

$$\kappa = \frac{\langle \sigma u \rangle}{M_x}, \tag{2}$$

where $\sigma$ is the cross-section for annihilation, $u$ is the mean particle velocity, and $M_x$ is the mass of the DM particle. Compared to the usual fluid equation, the effective pressure term is

$$P = \frac{\kappa\rho^2 - \Psi}{3H}. \tag{3}$$

When $\kappa\rho^2 - \Psi < 0$, what means that the IDM particle creation term is larger than the annihilation item, IDM may serve as a negative pressure source in the global dynamics of the Universe, like the role of Dark Energy in the general cosmological models.

Basilakos & Plionis (2009) identified two functional forms for which the previous Boltzmann equation can be solved analytically. Refering to Appendix B in Basilakos & Plionis (2009), only one of these two is of interest because it provides a "$\propto a^{-3}$" dependence of the scale factor, which is

$$\Psi(a) = aH(a)R(a) = C_1(n+3)a^n H(a) + \kappa C_1^2 a^{2m}. \tag{4}$$

And the total energy density is

$$\rho(a) = C_1 a^n + \frac{a^{-3}F(a)}{C_2 - \int_1^a x^{-3} f(x)F(x)\mathrm{d}x}, \tag{5}$$

where $f(a) = -\kappa/[aH(a)]$, and the kernal function $F(a)$ has the form

$$F(a) = \exp\left[-2\kappa C_1 \int_1^a \frac{x^{n-1}}{H(x)}\mathrm{d}x\right]. \tag{6}$$

The first term of Eq.(5) is the density corresponding to the residual matter creation that results from a possible disequilibrium between the particle creation and annihilation processes, while the second term can be viewed as the energy density of the self-IDM particles that are dominated by the annihilation process.

### 2.1. *Model 1: relation to the ΛCDM model*

If $n = 0$, the global density evolution can be transformed as

$$\rho(a) = C_1 + a^{-3}\frac{e^{-2\kappa C_1(t-t_0)}}{C_2 - \kappa Z(t)}, \tag{7}$$

where $Z(t) = \int_{t_0}^{t} a^{-3} e^{-2\kappa C_1 (t'-t_0)} \mathrm{d}t'$ (Basilakos & Plionis (2009)). Using the usual unit-less $\Omega$-like parameterization, we obtain that

$$\left(\frac{H}{H_0}\right)^2 = \Omega_{1,0} + \frac{\Omega_{1,0}\Omega_{2,0} a^{-3} e^{-2\kappa C_1 (t-t_0)}}{\Omega_{1,0} + \kappa C_1 \Omega_{2,0} Z(t)}, \quad (8)$$

where $\Omega_{1,0} = 8\pi G C_1/3H_0^2$ and $\Omega_{2,0} = 8\pi G/3H_0^2 C_2$, which related to $\Omega_\Lambda$ and $\Omega_m$ in the $\Lambda$CDM model, respectively. From Eq.(2), we can also give the mass of the DM particle related to the range of $\kappa C_1$(in the unit of $\mathrm{Gyr}^{-1}$)

$$M_x = \frac{3.325 \times 10^{-12}}{\kappa C_1} \frac{\langle \sigma u \rangle}{10^{-23}} h^2 (1 - \Omega_{2,0})\, \mathrm{GeV}, \quad (9)$$

where $h \equiv H_0/[100\mathrm{km/s/Mpc}]$.

### 2.2. *Model 2 : relation to the wCDM model*

If $\kappa = 0$, the global density evolution can be written as

$$\rho(a) = \mathcal{D} a^{-3} + C_1 a^n, \quad (10)$$

where $\mathcal{D} = C_2 - C - 1$. The conditions in which the current model acts as a quintessence cosmology are given by $\mathcal{D} > 0, C_1 > 0$, and $w_{\mathrm{IDM}} = -1 - n/3$. This solution is mathematically equivalent to that of the gravitational matter creation model of(). The Hubble flow is now given by

$$\left(\frac{H}{H_0}\right)^2 = \Omega_{2,0} a^{-3} + \Omega_{1,0} a^n, \quad (11)$$

where $\Omega_{2,0} = 8\pi G\mathcal{D}/3H_0^2$ and $\Omega_{1,0} = 8\pi G C_1/3H_0^2$, respectively.(Basilakos & Plionis (2009))

## 3. DATASET

To constrain the relevant IDM models (Basilakos & Plionis (2009)), we use the newly revised observational $H(z)$ data (OHD)(Simon et al. (2005); Stern et al. (2010); Moresco et al. (2012); Zhang et al. (2014); Moresco et al. (2016); Ratsimbazafy et al. (2017); Moresco (2015); Borghi et al. (2022); Jiao et al. (2023)), the Pantheon+ set of 1701 SNe Ia (Scolnic et al. (2022)), the quasar data from Lusso, E. et al. (2020), the BAO data from SDSS and DESI 2024.

### 3.1. *The observational H(z) data*

It is widely known that the Hubble parameter $H(z)$ depends on the differential age as a function of redshift $z$ in the form

$$H(z) = -\frac{1}{1+z}\frac{\mathrm{d}z}{\mathrm{d}t}, \quad (12)$$

which provides a direct measurement on $H(z)$ based on $\mathrm{d}z/\mathrm{d}t$. OHD measurements have recently been acquired mainly employing cosmic chronometers (CC). The CC method is used to provide 33 observational data points, which are taken in the redshift range [0.07, 1.965]. The Table 1 lists the OHD dataset used in this analysis. In this case, $\chi^2$ can be defined as

$$\chi^2_{\mathrm{OHD}} = \sum_i^{33} \frac{(H_{\mathrm{th}} - H_{\mathrm{data}})^2}{\sigma_i^2}. \quad (13)$$

**Table 1.** The OHD dataset

| $z$ | $H(z)$ | Reference |
|---|---|---|
| 0.07 | 69±19.6 | Zhang et al. (2014) |
| 0.09 | 69±12 | Simon et al. (2005) |
| 0.12 | 68.6±26.2 | Zhang et al. (2014) |
| 0.17 | 83±8 | Simon et al. (2005) |
| 0.179 | 75±4 | Moresco et al. (2012) |
| 0.199 | 75±5 | Moresco et al. (2012) |
| 0.2 | 72.9±29.6 | Zhang et al. (2014) |
| 0.27 | 77±14 | Simon et al. (2005) |
| 0.28 | 88.8±36.6 | Zhang et al. (2014) |
| 0.352 | 83±14 | Moresco et al. (2012) |
| 0.3802 | 83±13.5 | Moresco et al. (2016) |
| 0.4 | 95±17 | Simon et al. (2005) |
| 0.4004 | 77±10.2 | Moresco et al. (2016) |
| 0.4247 | 87.1±11.2 | Moresco et al. (2016) |
| 0.4497 | 92.8±12.9 | Moresco et al. (2016) |
| 0.47 | 89±34 | Ratsimbazafy et al. (2017) |
| 0.4783 | 80.9±9 | Moresco et al. (2016) |
| 0.48 | 97±62 | Stern et al. (2010) |
| 0.593 | 104±13 | Moresco et al. (2012) |
| 0.68 | 92±8 | Moresco et al. (2012) |
| 0.75 | 98.8±33.6 | Borghi et al. (2022) |
| 0.781 | 105±12 | Moresco et al. (2012) |
| 0.8 | 113.1±15.1 | Jiao et al. (2023) |
| 0.875 | 125±17 | Moresco et al. (2012) |
| 0.88 | 90±40 | Stern et al. (2010) |
| 0.9 | 117±23 | Simon et al. (2005) |
| 1.037 | 154±20 | Moresco et al. (2012) |
| 1.3 | 168±17 | Simon et al. (2005) |
| 1.363 | 160±33.6 | Moresco (2015) |
| 1.43 | 177±18 | Simon et al. (2005) |
| 1.53 | 140±14 | Simon et al. (2005) |
| 1.75 | 202±40 | Simon et al. (2005) |
| 1.965 | 186.5±50.4 | Moresco (2015) |

### 3.2. *Type Ia supernovae*

SNe Ia have long been used as "standard candles" to give a direct measurement of their luminosity distance,

and provides strong constraints on cosmological parameters. We use the latest Pantheon+ data set of 1701 SNe Ia samples(Scolnic et al. (2022)), which covers the redshift range [0, 2.26].

We use the fiducial SN Ia magnitude ($M_b$) determined from SH0ES 2021 Cepheid host distances(Riess et al. (2022)), which gives the $\mu_{\rm data}$ and we give the $\chi^2$ as

$$\chi^2_{\rm SNe} = \Delta^{\rm T} C^{-1} \Delta, \tag{14}$$

where $\Delta = (\mu_{\rm th} - \mu_{\rm data})$ and $C^{-1}$ is the inverse of the covariance matrix of the SNe Ia data, the distance modulus is $\mu = 5\log_{10}(d_L/{\rm Mpc}) + 25$, and the luminosity distance $d_L$ can be given as a function of redshift $z$

$$d_L = (1+z)\int_0^z \frac{c{\rm d}z'}{H(z')}. \tag{15}$$

To eliminate the advanced restriction to $H_0$ from $M_b$, we adopt the likelihood function as

$$\widetilde{\chi}^2_{\rm SNe} = \chi^2_{\rm SNe} - \frac{B^2}{C} + \ln\left(\frac{C}{2\pi}\right), \tag{16}$$

where $B = \Delta^{\rm T} C^{-1}$ and $C$ is the sum of $C^{-1}$. Apparently these two functions give the same constraints in $\Omega_{2,0}$ and $\log_{10}(\kappa C_1)$.

### 3.3. *Quasar*

The quasar gives a higher redshift than SNe Ia. We use the QSO dataset from Lusso, E. et al. (2020), which gives 2421 samples with the ultraviolet (UV) and X-ray luminosity. The redshift is up to $\simeq 7.5$.

The $L_X - L_{UV}$ relation of quasar is usually written as

$$\log_{10}(L_X) = \beta + \gamma\log_{10}(L_{UV}), \tag{17}$$

which gives that

$$\begin{aligned}\log_{10}(F_X) = \beta + (\gamma-1)\log_{10}(4\pi) + \gamma\log_{10}(F_{UV}) \\ +2(\gamma-1)\log_{10}(d_L),\end{aligned} \tag{18}$$

where $d_L$ is the luminosity distance same as Eq.(15). Here we use the parameters defined in Li et al. (2024), which gives

$$\beta = \beta_0 + \beta_1(1+z), \gamma = \gamma_0 + \gamma_1(1+z), \tag{19}$$

so the $\chi^2$ function for the QSO data can be defined as

$$\chi^2_{\rm QSO} = \sum_i^{2421}\left[\frac{(y^2_{\rm th} - y^2_{\rm data})}{s_i^2} - \ln(2\pi s_i^2)\right], \tag{20}$$

where $s_i^2 = {\rm d}y_i^2 + \gamma^2{\rm d}x_i^2 + \delta^2$ refers to the uncertainties on the $x_i$ ($\log_{10}F_X$) and $y_i$ ($\log_{10}F_{UV}$) and $\delta_i$ reprensent the instrinsic dispersion.

### 3.4. *Baryon acoustic oscillation*

The Baryon acoustic oscillation method (BAO) provides a key cosmological probe sensitive to the cosmic expansion history with well-controlled systematics. We use two BAO data sets from the SDSS(Alam et al. (2021)) and DESI 2024(Collaboration et al. (2024)), which are given at Table 2 and Table 3, respectively. The redshift is up to 2.33 both in the SDSS and the DESI 2024 dataset.

The $\chi^2$ function for the BAO data is defined as

$$\chi^2_{\rm BAO} = \sum_i \frac{(D_{\rm th}/r_{\rm d} - D_{\rm data}/r_{\rm d})^2}{\sigma_i^2}, \tag{21}$$

where $D$ refers to $D_{\rm M}$, $D_{\rm H}$, or $D_{\rm V}$, which ara given as

$$D_{\rm M}(z) = c\int_0^z \frac{{\rm d}z'}{H(z')}, \tag{22}$$

$$D_{\rm H}(z) = \frac{c}{H(z)}, \tag{23}$$

$$D_{\rm V}(z) = \left[zD^2_{\rm M}(z)D_{\rm H}(z)\right]^{1/3}, \tag{24}$$

and $r_{\rm d}$ is the sound horizon at the drag epoch, which is given as

$$r_{\rm d} = \int_{z_{\rm drag}}^{\infty} \frac{c_s(z'){\rm d}z'}{H(z')}, \tag{25}$$

where $c_s$ is the sound speed prior to recombination.

However, the solution of Eq.(8) only gives an upper limit of redshift $z_{\rm max}$ (see Appendix), and we just try to use the cross parameter $r_{\rm d}h$ to give the constraints.

**Table 2.** The BAO-only dataset from SDSS

| $z_{\rm eff}$ | $D_{\rm M}/r_{\rm d}$ | $D_{\rm H}/r_{\rm d}$ | $D_{\rm V}/r_{\rm d}$ |
|---|---|---|---|
| 0.15 | | | 4.47±0.17 |
| 0.38 | 10.23±0.17 | 25±0.76 | |
| 0.51 | 13.36±0.21 | 22.33±0.58 | |
| 0.7 | 17.86±0.33 | 19.33±0.53 | |
| 0.85 | | | $18.33^{+0.57}_{-0.62}$ |
| 1.48 | 30.69±0.8 | 13.26±0.55 | |
| 2.33 | 37.6±1.9 | 8.93±0.28 | |
| 2.33 | 37.3±1.7 | 9.08±0.34 | |

## 4. CONSTRAINT RESULTS

We use the Markov chain Monte Carlo (MCMC) method based on the opening package `emcee` to give a global constraints to the free parameters $\Omega_{2,0}$ and $\log_{10}(\kappa C_1)$ in Model 1 and $n$ in Model 2. Besides, we also add the parameter $H_0$ or $h$ to give the constraints to the dark matter particle mass $M_x$.

The prior range set for free parameters are given at Table 4

**Table 3.** The BAO dataset from DESI 2024

| $z_{\rm eff}$ | $D_{\rm M}/r_{\rm d}$ | $D_{\rm H}/r_{\rm d}$ | $D_{\rm V}/r_{\rm d}$ |
|---|---|---|---|
| 0.295 | | | 7.93±0.15 |
| 0.51 | 13.62±0.25 | 20.98±0.61 | |
| 0.706 | 16.85±0.32 | 20.08±0.6 | |
| 0.93 | 21.71±0.28 | 17.88±0.35 | |
| 1.317 | 27.79±0.69 | 13.82±0.42 | |
| 1.491 | | | 26.07±0.67 |
| 2.33 | 39.71±0.94 | 8.52±0.17 | |

**Table 4.** Parameters and priors used in analysis

| parameter | initial | prior |
|---|---|---|
| $\Omega_{2,0}$ | 0.3 | $\mathcal{U}[0.0, 1.0]$ |
| $n$ | 0 | $\mathcal{U}[-10, 10]$ |
| $\log_{10}(\kappa C_1/\mathrm{Gyr}^{-1})$ | — | $\mathcal{U}[-10, 0]$ |
| $H_0$[km/s/Mpc] | 70 | $\mathcal{U}[60, 80]$ |
| $\beta_0$ | 6 | $\mathcal{U}[-15, 15]$ |
| $\beta_1$ | 1 | $\mathcal{U}[-10, 10]$ |
| $\gamma_0$ | 0.6 | $\mathcal{U}[0.0, 1.0]$ |
| $\gamma_1$ | 0 | $\mathcal{U}[-1.0, 1.0]$ |
| $\delta$ | 0.2 | $\mathcal{U}[0.0, 1.0]$ |
| $r_{\rm d}h$[Mpc] | 100 | $\mathcal{U}[50, 150]$ |

### 4.1. *Model 1: mimicking the ΛCDM model*

The Eq.(8) convergant to the flat ΛCDM model as $\log_{10}(\kappa C_1) \to -\infty$, therefore the constraints could only give the upper limit of what, and give the lower limit of $M_x$ according to Eq.(9), respectively.

We use the 97.7% and 2.3% quantiles (about $2\sigma$) to determine the upper and lower limits of the parameters, and the results are shown in Table 5.

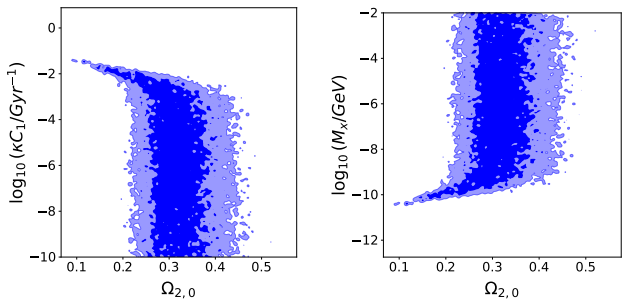


**Figure 1.** The constraint result from the observational $H(z)$ data

We would find that the SNe Ia and QSO combined result is most similar to SNe Ia result, what may refer that the QSO cannot give an effective constraint. It may be due to the data quality at the high redshift.

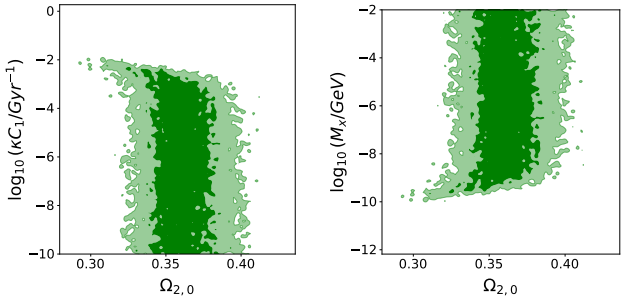


**Figure 2.** The constraint result from the supernovae Ia data

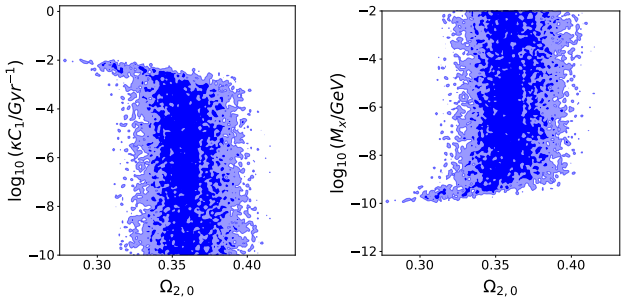


**Figure 3.** The constraint result from the SNe Ia + QSO data

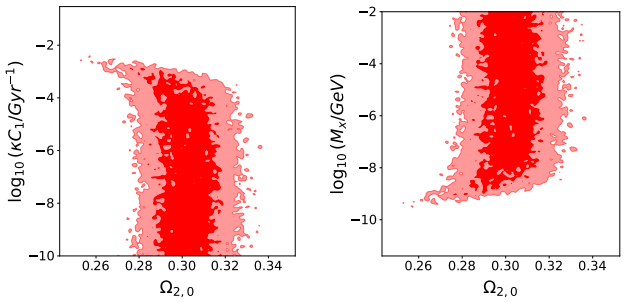


**Figure 4.** The constraint result from the BAO data

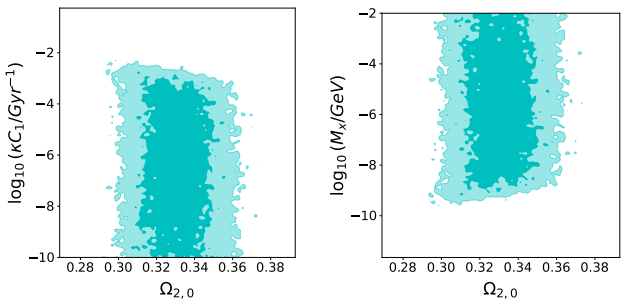


**Figure 5.** The constraint result from the OHD + SNe Ia data

**Table 5.** The constraint results of Model 1

| Model 1 | OHD | SNe Ia | SNe Ia + QSO | BAO | OHD + SNe Ia | OHD + SNe Ia + BAO |
|---|---|---|---|---|---|---|
| $\Omega_{2,0}$ | $0.321^{+0.055}_{-0.067}$ | $0.360^{+0.020}_{-0.020}$ | $0.359^{+0.020}_{-0.020}$ | $0.301^{+0.013}_{-0.013}$ | $0.330^{+0.016}_{-0.016}$ | $0.313^{+0.010}_{-0.010}$ |
| $\log_{10}(\kappa C_1/\mathrm{Gyr}^{-1})$ | $< -2.17$ | $< -2.51$ | $< -2.57$ | $< -3.10$ | $< -2.88$ | $< -3.39$ |
| $\log_{10}(M_x/\mathrm{GeV})$ | $> -9.77$ | $> -9.42$ | $> -9.40$ | $> -8.84$ | $> -9.03$ | $> -8.52$ |

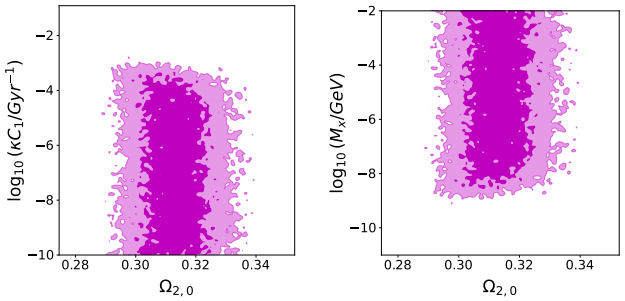


**Figure 6.** The constraint result from the OHD + SNe Ia + BAO data

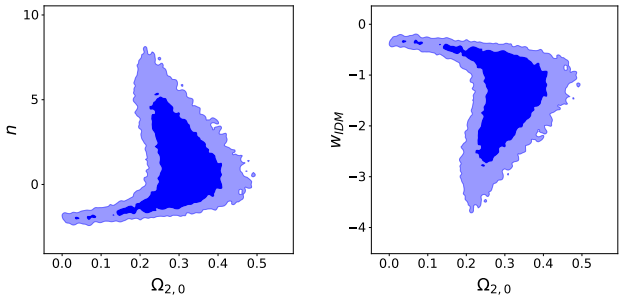


**Figure 7.** The constraint result from the observational $H(z)$ data

### 4.2. *Model 2: mimicking the wCDM model*

The constraint results of Model 2 are shown in Table 6.

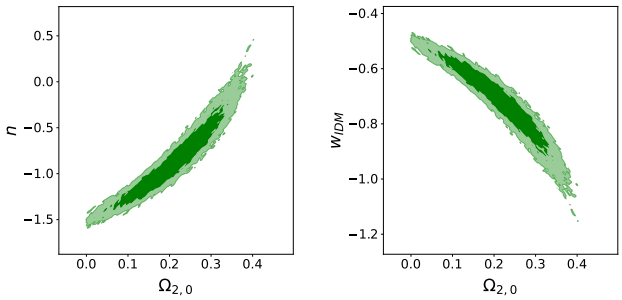


**Figure 8.** The constraint result from the supernovae Ia data

The results from three dataset are different

## 5. CONCLUSIONS

## APPENDIX

## A. THE THEORETICAL SOLUTION OF MODEL 1

Apply the Eq.(12) to Eq.(8), we can get a simple nonlinear second-order differential equation for the redshift $z(t)$, which can be written as

$$2H_0^2\Omega_{1,0}(1+z)^2z'z''+\kappa C_1z'^4-5H_0^2\Omega_{1,0}(1+z)z'^3+3H_0^4\Omega_{1,0}^2(1+z)^3z'-H_0^4\Omega_{1,0}^2\kappa C_1[(z+1)^4-1]=H_0^4\Omega_{1,0}^2\kappa C_1, \quad \text{(A1)}$$

where the prime denotes the derivative with respect to $t$. The equation can be simplified as

$$2H_0^2\Omega_{1,0}y^2y'y''+\kappa C_1y'^4-5H_0^2\Omega_{1,0}yy'^3+3H_0^4\Omega_{1,0}^2y^3y'-H_0^4\Omega_{1,0}^2\kappa C_1y^4=0, \quad \text{(A2)}$$

where $y=z+1$, now it is a homogeneous function and we can give the general solution as $y=\exp f$ with $f$ a function of $t$, the equation now is

$$2H_0^2\Omega_{1,0}f'f''+\kappa C_1f'^4-3H_0^2\Omega_{1,0}f'^3+3H_0^4\Omega_{1,0}^2f'-H_0^4\Omega_{1,0}^2\kappa C_1=0. \quad \text{(A3)}$$

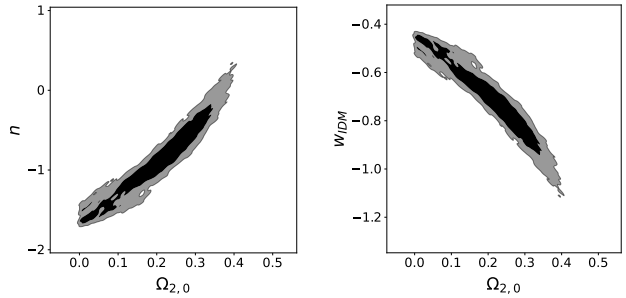


**Figure 9.** The constraint result from the SNe Ia + QSO data

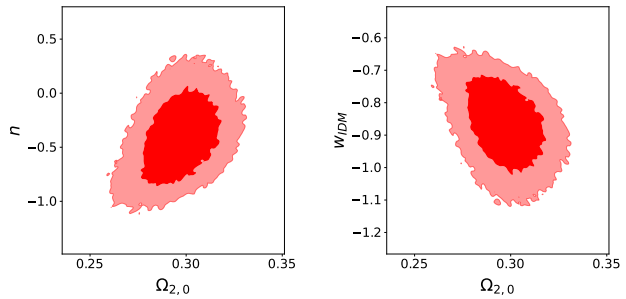


**Figure 10.** The constraint result from the BAO data

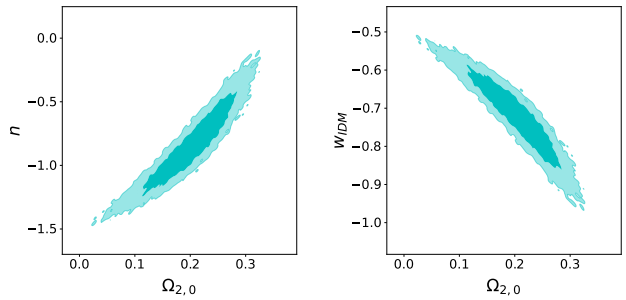


**Figure 11.** The constraint result from the OHD + SNe Ia data

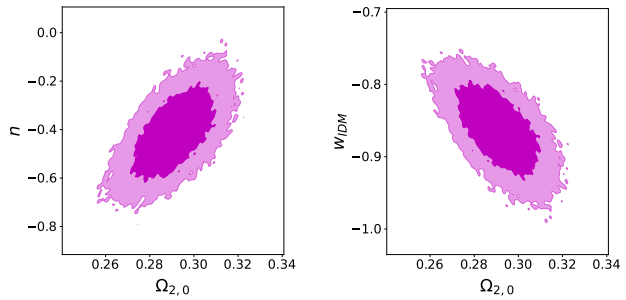


**Figure 12.** The constraint result from the OHD + SNe Ia + BAO data

**Table 6.** The constraint results of Model 2

| Model 2 | OHD | SNe Ia | SNe Ia + QSO | BAO | OHD + SNe Ia | OHD + SNe Ia + BAO |
|---|---|---|---|---|---|---|
| $\Omega_{2,0}$ | $0.295^{+0.077}_{-0.077}$ | $0.216^{+0.096}_{-0.078}$ | $0.208^{+0.12}_{-0.087}$ | $0.296^{+0.014}_{-0.014}$ | $0.202^{+0.060}_{-0.049}$ | $0.291^{+0.013}_{-0.013}$ |
| $n$ | $1.4^{+1.4}_{-2.8}$ | $-0.82^{+0.29}_{-0.44}$ | $-0.85^{+0.42}_{-0.49}$ | $-0.40^{+0.29}_{-0.29}$ | $-0.83^{+0.24}_{-0.27}$ | $-0.41^{+0.13}_{-0.13}$ |
| $w_{\rm IDM}$ | $-1.5^{+0.5}_{-0.9}$ | $-0.73^{+0.10}_{-0.15}$ | $-0.72^{+0.14}_{-0.16}$ | $-0.87^{+0.10}_{-0.10}$ | $-0.72^{+0.09}_{-0.09}$ | $-0.86^{+0.04}_{-0.04}$ |

We use $g = f'$, which also gives $g(t) = y'/y = -H(t)$, then the equation can be written as

$$2H_0^2\Omega_{1,0}gg' + \kappa C_1 g^4 - 3H_0^2\Omega_{1,0}g^3 + 3H_0^4\Omega_{1,0}^2 g - H_0^4\Omega_{1,0}^2\kappa C_1 = 0. \tag{A4}$$

It can be theoretically solved and the solution is like

$$g(t) = \mathcal{G}\left(-\frac{t}{2H_0^2\Omega_{1,0}} + Const\right), \tag{A5}$$

where $\mathcal{G}$ is the inverse function of

$$\mathcal{F}(x) = \frac{3H_0\sqrt{\Omega_{1,0}}\text{arctanh}\frac{x}{H_0\sqrt{\Omega_{1,0}}} - \kappa C_1\log(x^2 - H_0^2\Omega_{1,0}) + \kappa C_1\log(\kappa C_1 x^2 - 3H_0^2\Omega_{1,0}x + H_0^2\Omega_{1,0}\kappa C_1)}{9H_0^4\Omega_{1,0}^2 - 4H_0^2\Omega_{1,0}(\kappa C_1)^2}. \tag{A6}$$

In this term, $\text{arctanh}(x) \doteq \frac{1}{2}\log\left(\frac{x+1}{x-1}\right)$ when $x < -1$, and the $Const$ is determined by the boundary condition $g(0) \to -\infty$, which is

$$Const = \mathcal{F}(-\infty) \equiv \lim_{x\to-\infty}\mathcal{F}(x) = \frac{\kappa C_1\ln\kappa C_1}{9H_0^4\Omega_{1,0}^2 - 4H_0^2\Omega_{1,0}(\kappa C_1)^2}. \tag{A7}$$

The initial time of today $t_0$ can be easily given as

$$t_0 = 2H_0^2\Omega_{1,0}[\mathcal{F}(-\infty) - \mathcal{F}(-H_0)], \tag{A8}$$

and the redshift $z_{\rm max}$ can be calculated as

$$z_{\rm max} = \exp\left[2H_0^2\Omega_{1,0}\int_{-\infty}^{-H_0}[\mathcal{F}(-\infty) - \mathcal{F}(x)]\mathrm{d}x + H_0 t_0\right] - 1, \tag{A9}$$

and $z_{\rm max}$ is also a function of $\Omega_{2,0}, \kappa C_1$ and $H_0$.

## REFERENCES


Alam, S., Aubert, M., Avila, S., et al. 2021, Phys. Rev. D, 103, 083533, doi: 10.1103/PhysRevD.103.083533

Basilakos, S., & Plionis, M. 2009, A&A, 507, 47, doi: 10.1051/0004-6361/200912661

Bennett, C. L., Banday, A. J., Górski, K. M., et al. 1996, The Astrophysical Journal, 464, L1, doi: 10.1086/310075

Borghi, N., Moresco, M., & Cimatti, A. 2022, The Astrophysical Journal Letters, 928, L4, doi: 10.3847/2041-8213/ac3fb2

Collaboration, D., Adame, A. G., Aguilar, J., et al. 2024, DESI 2024 VI: Cosmological Constraints from the Measurements of Baryon Acoustic Oscillations. https://arxiv.org/abs/2404.03002

Eisenstein, D. J., Zehavi, I., Hogg, D. W., et al. 2005, The Astrophysical Journal, 633, 560, doi: 10.1086/466512

Jiao, K., Borghi, N., Moresco, M., & Zhang, T.-J. 2023, The Astrophysical Journal Supplement Series, 265, 48, doi: 10.3847/1538-4365/acbc77

Li, X., Keeley, R. E., & Shafieloo, A. 2024, Redshift evolution of the X-ray and UV luminosity relation of quasars: calibrated results from SNe Ia. https://arxiv.org/abs/2408.15547

Lusso, E., Risaliti, G., Nardini, E., et al. 2020, A&A, 642, A150, doi: 10.1051/0004-6361/202038899

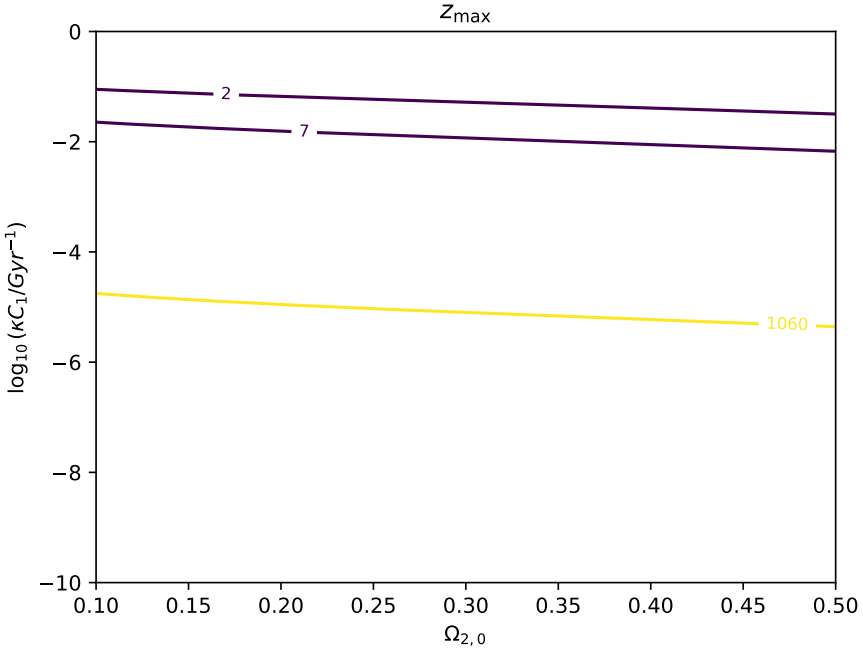


**Figure 13.** The redshift $z_{\max}$ as $H_0 = 70$ km/s/Mpc


Moresco, M. 2015, Monthly Notices of the Royal Astronomical Society: Letters, 450, L16, doi: 10.1093/mnrasl/slv037

Moresco, M., Cimatti, A., Jimenez, R., et al. 2012, Journal of Cosmology and Astroparticle Physics, 2012, 006, doi: 10.1088/1475-7516/2012/08/006

Moresco, M., Pozzetti, L., Cimatti, A., et al. 2016, Journal of Cosmology and Astroparticle Physics, 2016, 014, doi: 10.1088/1475-7516/2016/05/014

Perlmutter, S., Aldering, G., Goldhaber, G., et al. 1999, The Astrophysical Journal, 517, 565, doi: 10.1086/307221

Ratsimbazafy, A. L., Loubser, S. I., Crawford, S. M., et al. 2017, Monthly Notices of the Royal Astronomical Society, 467, 3239, doi: 10.1093/mnras/stx301

Riess, A. G., Filippenko, A. V., Challis, P., et al. 1998, The Astronomical Journal, 116, 1009, doi: 10.1086/300499

Riess, A. G., Yuan, W., Macri, L. M., et al. 2022, The Astrophysical Journal Letters, 934, L7, doi: 10.3847/2041-8213/ac5c5b

Scolnic, D., Brout, D., Carr, A., et al. 2022, The Astrophysical Journal, 938, 113, doi: 10.3847/1538-4357/ac8b7a

Simon, J., Verde, L., & Jimenez, R. 2005, Phys. Rev. D, 71, 123001, doi: 10.1103/PhysRevD.71.123001

Stern, D., Jimenez, R., Verde, L., Kamionkowski, M., & Stanford, S. A. 2010, Journal of Cosmology and Astroparticle Physics, 2010, 008, doi: 10.1088/1475-7516/2010/02/008

Zhang, C., Zhang, H., Yuan, S., et al. 2014, Research in Astronomy and Astrophysics, 14, 1221, doi: 10.1088/1674-4527/14/10/002